

# The Significance of Simple Invariant Solutions in Turbulent Flows

GENTA KAWAHARA

Graduate School of Engineering Science, Osaka University, Toyonaka, Osaka  
560-8531, Japan; email: kawahara@me.es.osaka-u.ac.jp

MARKUS UHLMANN

Institute for Hydromechanics, Karlsruhe Institute of Technology, 76128  
Karlsruhe, Germany; email: uhlmann@kit.edu

LENNAERT VAN VEEN

Faculty of Science, University of Ontario Institute of Technology, Oshawa ON  
L1H 7K4, Canada; email: Lennaert.vanVeen@uoit.ca

*Annual Review of Fluid Mechanics*, **44**, 2012. In press.

**Key Words** turbulence, dynamical system, coherent structure, turbulence statistics

**Abstract** Recent remarkable progress in computing power and numerical analysis is enabling us to fill a gap in the dynamical systems approach to turbulence. One of the significant advances in this respect has been the numerical discovery of simple invariant sets, such as nonlinear equilibria and periodic solutions, in well-resolved Navier–Stokes flows. This review describes some fundamental and practical aspects of dynamical systems theory for the investigation of turbulence, focusing on recently found invariant solutions and their significance for the dynamical and statistical characterization of low-Reynolds-number turbulent flows. It is shown that the near-wall regeneration cycle of coherent structures can be reproduced by such solutions. The typical similarity laws of turbulence, i.e. the Prandtl wall law and the Kolmogorov law for the viscous range, as well as the pattern and intensity of turbulence-driven secondary flow in a square duct can also be represented by these simple invariant solutions.

## CONTENTS

INTRODUCTION . . . . .	1
DYNAMICAL SYSTEMS . . . . .	2
<i>Invariant Solutions</i> . . . . .	3
<i>Connecting Orbits</i> . . . . .	3
<i>Computation and Continuation of Invariant Solutions</i> . . . . .	4
<i>SIDEBAR: Detection of Unstable Invariant Sets</i> . . . . .	5
SIMPLE INVARIANT SOLUTIONS . . . . .	5
<i>Steady and Travelling-Wave Solutions</i> . . . . .	5
<i>Periodic Solutions</i> . . . . .	7
<i>Comparison of Solutions</i> . . . . .	8
SIGNIFICANCE OF INVARIANT SOLUTIONS . . . . .	9
<i>Near-Wall Regeneration Cycle</i> . . . . .	9
<i>Turbulence Statistics for the Viscous Range</i> . . . . .	10
<i>Mean Secondary Flow</i> . . . . .	11
FUTURE DIRECTIONS . . . . .	13

## 1 INTRODUCTION

In 1983 the IUTAM (International Union of Theoretical and Applied Mechanics) Symposium on Turbulence and Chaotic Phenomena in Fluids was held in Kyoto, Japan. At that symposium a French participant showed a transparency on which a cartoon was drawn of two corps ready to do battle against each other (see Yamada 2002). One was the “traditional statistical theory” army which claimed that turbulence should be considered statistically while the other was “chaos” army which insisted that turbulence could be described as deterministic chaos in terms of dynamical systems theory. In that period the new concept of chaos was starting to have a strong impact on a variety of disciplines in science and engineering, including turbulence research. The above anecdote is an indication of the expectation that dynamical systems theory would be a counterpart of the statistical theory of turbulence, although there was a wide gap between the low-dimensional chaotic systems discussed at that time and turbulent flow. Recently, however, nonlinear equilibrium and periodic solutions to the full Navier–Stokes equation have been found numerically in several flow systems, and it has turned out that they are significant for a theoretical description of not only transition to turbulence but also fully turbulent flow. This paper is devoted to a review of recently reported dynamical systems approaches to the problem of low-Reynolds-number turbulence based on such equilibrium and periodic solutions. Several review articles have recently appeared concerning the dynamical systems approach to the transition to turbulence (see Eckhardt et al. 2008, 2007, Kerswell 2005). Here we focus our attention on fully turbulent flow.

Although apparently infinite-dimensional, the turbulent motion of a viscous fluid governed by the Navier–Stokes equations, i.e., by a set of partial differential evolution equations in a finite domain, is a finite-dimensional dynamical system. Physically, the reason is that small-scale motions are smoothed by viscosity. There is a mathematical proof of the existence of approximate inertial manifolds for the Navier–Stokes equations that provides a relation between the dominant modes and the higher-order ones that can be truncated (see, e.g. Foias et al. 2001). Within such a manifold, the Navier–Stokes equations can be approximated by a finite-dimensional system of ODEs (Ordinary Differential Equations). For example, Keefe et al. (1992) demonstrated numerically that a spatially periodic turbulent channel flow simulated with a spatial resolution of  $16 \times 33 \times 16$  at the friction Reynolds number  $Re_\tau = 80$  was really confined to a finite-dimensional strange attractor whose Kaplan–Yorke dimension was estimated to be 780. The Kaplan–Yorke dimension specifies dimension of a volume element in phase space which neither expands nor shrinks on average over time.

Dynamical systems theory tells us that coherent structures in turbulent flows may be thought of as low-dimensional invariant sets in phase space, in the neighbourhood of which the system spends a substantial fraction of time, as suggested by Jiménez (1987). Spatio-temporally organized structures appear when a turbulent state approaches such an invariant set. Possible invariant solutions are simple saddles in phase space, such as steady travelling waves, or time-periodic solutions. It is known that the statistical properties of chaotic low-dimensional dynamical systems can be estimated from the coherent states represented by unstable periodic orbits (Artuso et al. 1990a,b, Christiansen et al. 1997, Cvitanović 1987). In this review, we will restrict ourselves to such relatively simple invariant solutions, even though coherent structures can also correspond to more complex

sets, such as the strange attractors of some highly reduced dynamical systems obtained from the Navier–Stokes equations by proper orthogonal decomposition (see, e.g. Holmes et al. 1996).

The fundamentals of dynamical systems theory are described in Section 2, including recent work on computational algorithms. In Section 3 we briefly review recently found simple invariant solutions for wall-bounded shear flows, such as plane Couette, plane Poiseuille, Hagen–Poiseuille and square-duct systems, and for triply periodic flow, namely Kida–Pelz flow (Kida 1985). We discuss the significance of the invariant solutions in dynamical and statistical descriptions of low-Reynolds-number turbulent flows in Section 4. The paper is concluded with an outlook for the dynamical system approach to turbulence and its open issues in Section 5.

## 2 DYNAMICAL SYSTEMS

As argued above, viscous flow can be approximated by a system of ODEs. The number of degrees of freedom this system comprises determines the spatial resolution of the flow simulation. In order to simulate the flow accurately, we must take into account all spatial scales that carry significant energy and those which are responsible for its dissipation. It is known phenomenologically that the number of resolution elements grows with the Reynolds number  $Re$  as  $Re^{9/4}$  (Landau & Lifshitz 1959). For three-dimensional simulations of even weakly turbulent flows at  $Re \gtrsim 10^2$  we should work on systems of ODEs with upward from  $10^5$  degrees of freedom. Here, we will discuss some of the theory and practice of analysing such systems.

In order to apply dynamical systems theory to fluid flow simulations, we reformulate the governing equations as

$$\frac{d\mathbf{x}}{dt} = \mathbf{f}(\mathbf{x}, \mathbf{p}), \quad (1)$$

where  $\mathbf{x}$  is the vector of dependent variables, for instance Fourier or Fourier-Chebyshev coefficients or components of the velocity at grid points. The vector field  $\mathbf{f}$  stems from the discretized Navier–Stokes equation and depends on parameters  $\mathbf{p}$ . In the context of the current review, these parameters determine the kinematic fluid viscosity  $\nu$ , the strength of forcing and the geometry of the flow domain. The vector  $\mathbf{x}$  lives in a “phase space” of dimension  $N$ , which usually coincides with  $\mathbb{R}^N$ . We denote the flow of this system of ODEs as  $\phi(\mathbf{x}, t; \mathbf{p})$ , such that for any fixed  $\mathbf{x}$ ,  $\phi(\mathbf{x}, t; \mathbf{p})$  is the solution which passes through point  $\mathbf{x}$  at  $t = 0$ . The Jacobian  $\mathbf{J} = \{\partial f_i / \partial x_j(\mathbf{x}; \mathbf{p})\}$  ( $1 \leq i, j \leq N$ ) plays a central role in the analysis of stability of solutions through the linearised equations

$$\frac{d\mathbf{A}}{dt} = \mathbf{J}\mathbf{A} \text{ (matrix form), or } \frac{d\mathbf{v}}{dt} = \mathbf{J}\mathbf{v} \text{ (vector form),} \quad (2)$$

where  $\mathbf{v} \in \mathbb{R}^N$  is a perturbation vector, i.e. a column vector of the fundamental matrix  $\mathbf{A}$ . For discretized Navier–Stokes equations, we typically have access only to a single perturbation vector in a simulation, either through a modification of the DNS (Direct Numerical Simulation) code to integrate the vector form of linearized equations (2) or through finite differences.

A practical remark is in place here. It can be quite a challenge to recast legacy software for the DNS of turbulence such that the vectors  $\mathbf{x}$ ,  $\mathbf{f}$  and  $\mathbf{p}$  can easily

be manipulated. The truly independent variables  $\mathbf{x}$  may have to be extracted from larger data structures taking into account boundary conditions and possible redundancy. Recently, DNS software has been written with an intuitive interface between the DNS and the dynamical systems formulation (see, for instance, the *channelflow* project by Gibson 2007).

## 2.1 Invariant Solutions

An important question that dynamical systems theory addresses concerns the long term behaviour of solutions to ODEs (1). Chaotic dynamics of a system can be decomposed into building blocks, namely simple invariant solutions and their stable and unstable manifolds.

The simplest invariant solution is an equilibrium, at which  $\mathbf{f}(\mathbf{x}, \mathbf{p}) = 0$ . Equilibria come in families, denoted by  $\bar{\mathbf{x}}(\mathbf{p})$ , which persist under changes of the parameters as long as the Jacobian,  $\mathbf{J}(\bar{\mathbf{x}}, \mathbf{p})$ , is not singular. Along a family, an eigenvalues of  $\mathbf{J}(\bar{\mathbf{x}}, \mathbf{p})$  may cross zero. In this case a saddle-node bifurcation occurs, at which two equilibria collide and disappear. If  $\mathbf{J}(\bar{\mathbf{x}}, \mathbf{p})$  has a pair of complex eigenvalues with zero real part, a Hopf bifurcation occurs, at which a periodic solution is created. Examples of both types of bifurcation were found in plane Couette flow by Clever & Busse (1997). If, and only if, the real part of all eigenvalues is negative, the equilibrium is stable. Nearby initial conditions will converge to it. A famous example is the laminar equilibrium in plane Couette flow. If the real part of some eigenvalues is positive, the equilibrium is a saddle. Examples of saddle-type equilibria are three-dimensional equilibrium states in plane Couette flow (Clever & Busse 1997, Nagata 1990).

The simplest time-dependent invariant solution is periodic. Any point  $\mathbf{x}'$  on a periodic solution satisfies  $\phi(\mathbf{x}', T; \mathbf{p}) = \mathbf{x}'$  and the smallest positive  $T$  for which this holds is called the period. Just like equilibria, periodic solutions come in families. Bifurcations and stability of such a family are determined by the Floquet multipliers, which are the eigenvalues of the monodromy matrix  $\mathbf{M} = \{\partial \phi_i / \partial x_j(\mathbf{x}', T; \mathbf{p})\}$  ( $1 \leq i, j \leq N$ ), i.e. the time- $T$  solution of the linearized equations (2). There is always one multiplier equal to unity, corresponding to perturbations along the periodic solution. A saddle-node bifurcation occurs if there is a second multiplier equal to unity. This happens, for instance, to the periodic solutions in plane Couette flow, identified by Kawahara & Kida (2001), when continued in the Reynolds number (Kawahara et al. 2006). A periodic solution is called a saddle if some of the multipliers are inside the unit circle in the complex plane and some are outside. The dynamical systems picture of turbulence suggests that infinitely many saddle-type periodic solutions exist and the state of the system wanders between them irregularly. This picture can be traced back all the way to Hopf (Cvitanović et al. 2010, Appendix A).

## 2.2 Connecting Orbits

Saddle-type invariant solutions regulate the global dynamics of a system through their stable and unstable manifolds. These manifolds are defined as the sets of initial conditions which converge to the saddles in positive and negative time, respectively (Wiggins 1990). At the equilibria and periodic solutions, the (un)stable manifold coincides with the subspace spanned by the (un)stable eigenvectors of the Jacobian and the monodromy matrix, respectively.

When a stable manifold intersects with an unstable manifold, the intersection contains at least one solution curve, called “homoclinic” if both manifolds are attached to the same saddle and “heteroclinic” if they are attached to different saddles. Such connecting orbits provide the pathways for the state of the system to wander from one saddle to another. Thus, with the dynamical systems picture of turbulence in mind, it is important to study connecting orbits. Computationally, this is a hard task. What we can decide purely on the basis of the stability properties of the saddles is the codimension of a connecting orbit, i.e. the number of parameters we need to tune in order for a connecting orbit to exist. The codimension  $c$  of an orbit connecting a saddle with an unstable manifold of dimension  $d_u$  to one with a stable manifold of dimension  $d_s$  is  $c = N - d_u - d_s + 1$ . For example, for a homoclinic orbit to an equilibrium we have  $d_u + d_s = N$  so  $c = 1$ , while for a homoclinic orbit to a periodic solution we have  $d_u + d_s = N + 1$  so  $c = 0$ . This means that we can only see orbits homoclinic to equilibria if we vary one system parameter, but we can expect to find orbits homoclinic to periodic solutions in a system with all parameters fixed.

### 2.3 Computation and Continuation of Invariant Solutions

The best available method for computing saddle-type invariant solutions is Newton iteration because of its quadratic convergence. Given an approximate equilibrium  $\bar{\mathbf{x}}_i$  we find a better approximation after the Newton step

$$\bar{\mathbf{x}}_{i+1} = \bar{\mathbf{x}}_i + \delta\mathbf{x}, \text{ where } \mathbf{J}(\bar{\mathbf{x}}_i, \mathbf{p}) \delta\mathbf{x} = -\mathbf{f}(\bar{\mathbf{x}}_i, \mathbf{p}) \quad (3)$$

The obvious difficulty is that we need to construct, store and factorise the  $N \times N$  Jacobian to solve this linear system. For periodic solution computations, the situation is even worse, since the fundamental matrix  $\mathbf{A}$  in the Newton step

$$\mathbf{x}'_{i+1} = \mathbf{x}'_i + \delta\mathbf{x}, \text{ where } [\mathbf{A}(\mathbf{x}'_i, T_i) - \mathbb{I}] \delta\mathbf{x} = -\boldsymbol{\phi}(\mathbf{x}'_i, T_i) + \mathbf{x}'_i \quad (4)$$

takes  $N$  integrations over time interval  $T_i$  to compute. Although some of the early computations were done using this approach (Kawahara et al. 2006, van Veen et al. 2006), in order to attain high spatial resolution it is necessary to switch to inexact linear solvers. Such methods construct an approximate solution to Newton step (3) or (4) on the basis of matrix-vector products, for the computation of which it suffices to integrate linearized equations (2) in the vector form. Most commonly used are Krylov subspace methods, in particular GMRES (Saad 2003). The efficiency of this methods depends on the eigenvalue structure of the matrix. If the eigenvalues are unfavourable, we need to precondition the linear problem (see, e.g. Tuckerman & Barkley 2000, for an example in Navier–Stokes flow). For periodic solutions, the linear problem is generally well conditioned. Sánchez et al. (2004) give an estimate of the number of necessary GMRES iterations in terms of bounds on the spectrum of  $\mathbf{M}$ . In their example computations, and many subsequent applications (e.g., Viswanath 2007), the number of GMRES iterations is less than 100 for  $N = O(10^5) - O(10^6)$ .

Continuation of invariant solutions in parameters takes only a small extension of the Newton–Krylov algorithm (see, e.g. Sánchez et al. 2004). The same Newton–Krylov method and preconditioner (if any) can be used (Dickson et al. 2007).

In the discussion above we have tacitly assumed that the dynamical system (1) has no symmetries. A discussion of symmetry, often important in turbulence, is

outside the scope of the current review. One important notion is that of relative equilibria (or travelling waves) and periodic solutions. These are observed as regular equilibria and periodic solutions in the appropriate moving coordinate frame, and their bifurcation theory and numerical treatment are analogous to those described above. A good starting point for the interested reader is Siminos & Cvitanović (2011).

## 2.4 SIDEBAR: Detection of Unstable Invariant Sets

Newton-Krylov iteration for the computation of invariant solutions requires an approximate solution to start with. Three methods for obtaining initial data have been used successfully for turbulent flows.

The first is one of bisection and generated most of the streak-dominated solutions discussed in Section 3.3. In flows with a stable laminar equilibrium, we consider two initial conditions, one leading to long-lived turbulence and one to quick laminarization. Bisection of initial conditions between these points yields orbits which closely approach near-laminar invariant solutions.

The second method is that of homotopy, and generated many of the solutions described in Section 3.1. An extra parameter is introduced in the system, for instance the amplitude of a body force. Invariant solutions may be found when changing this parameter and traced back to the original system by continuation.

The third method is one of filtering. Approximate recurrences or equilibria are filtered from a turbulent time series. Initial data thus obtained are usually coarse and necessitate globally convergent Newton methods. Dennis & Schnabel (1996) describes several variants which can be integrated with Krylov subspace methods. Lan & Cvitanović (2004) formulated a global Newton step for periodic solutions. Using their idea, Fazendeiro et al. (2010) computed periodic solutions in triply-periodic weak turbulence.

## 3 SIMPLE INVARIANT SOLUTIONS

Even using Krylov subspace algorithms, the numerical computation of simple invariant solutions in a large domain with inflow and outflow boundary conditions comparable to experiments is beyond our computational capabilities at this moment. However, DNS of turbulent states in periodic domains is known to reproduce the statistics of experiments well (see, e.g. Jiménez & Kawahara 2011). It is also known that at least part of the buffer layer is well represented even by the minimal flow units which Jiménez & Moin (1991) have determined by minimizing the streamwise and spanwise dimensions of a computational periodic box for plane Poiseuille turbulence. The same approach was later applied to plane Couette flow by Hamilton et al. (1995). Such reduced systems are small enough for their coherent structures to be described in terms of simple invariant solutions. In this section we see that several of these have been found for doubly- or singly-periodic minimal domains in plane Couette, Poiseuille, Hagen–Poiseuille and square-duct flows, and for triply-periodic Kida–Pelz flow.

### 3.1 Steady and Travelling-Wave Solutions

The first solutions of this kind were obtained by Nagata (1990) in plane Couette flow. That flow is stable to infinitesimal disturbances at all Reynolds numbers,

so that nonlinear solutions cannot simply be found by continuation from the laminar state. Nagata (1990) found his solution by the homotopy method, imposing a spanwise rotation on the system, which led to a sequence of bifurcations of two- and three-dimensional steady solutions from the laminar state. He then extended one of those three-dimensional nonlinear solutions to the non-rotating case. Clever & Busse (1992) obtained the same three-dimensional solution by imposing a temperature difference between the two horizontal walls of a Couette flow, and the same solution was again found by Waleffe (1998, 2003) who imposed an artificial body force (see Section 4.1). The three-dimensional equilibrium solution found by those three groups arises from a saddle-node bifurcation at a finite value of the Reynolds number, above which it splits into two solution branches. As shown in Figure 1, the solutions of the upper branch contain a wavy low-velocity streak flanked with a pair of staggered counter-rotating streamwise ( $x$ ) vortices. The solutions in the lower branch are roughly streamwise independent and closer to the laminar state. Other equilibrium solutions have been found more recently for Couette flow (Gibson et al. 2008, 2009, Itano & Generalis 2009, Nagata 1997, Schmiegell 1999). They are not necessarily related to the one originally identified by Nagata (1990), but they have been used to discuss coherent structures or the subcritical transition to turbulence.

In contrast to plane Couette flow, laminar Poiseuille flow in a plane channel is unstable to infinitesimal disturbances beyond a certain Reynolds number, from where a two-dimensional equilibrium travelling-wave solution bifurcates subcritically. A three-dimensional solution originating from that wave was found by Ehrenstein & Koch (1991), while Waleffe (1998, 2001, 2003) and Itano & Toh (2001) found families of three-dimensional steady travelling waves that are not known to be connected to the laminar state. In the case of Waleffe (1998, 2001, 2003), he used the homotopy approach to construct nonlinear steady travelling waves with a reflectional symmetry with respect to the channel central plane, which also contain streaks and vortices, and can be continuously connected to the Nagata (1990) solution for plane Couette flow (Waleffe 2003). As shown in Figure 2, the Waleffe solution for plane Poiseuille flow exhibits a pair of staggered streamwise vortices and an associated wavy streak. The solution found by Itano & Toh (2001) also includes streaks and vortices, but they are localized near one of the two walls. A three-dimensional steady travelling wave with a very similar structure was found by Jiménez & Simens (2001) in a so-called ‘autonomous’ flow that is confined to the vicinity of one wall under the action of a damping filter (Jiménez & Pinelli 1999).

The laminar Hagen–Poiseuille flow in a circular pipe is linearly stable at all Reynolds numbers, but Faisst & Eckhardt (2003) and Wedin & Kerswell (2004) have recently discovered three-dimensional steady travelling-wave solutions by using the homotopy approach proposed by Waleffe (1998, 2003). Both groups obtained the same solution, which possesses discrete rotational symmetry with respect to the pipe axis, with wavy low-velocity streaks flanked by staggered streamwise vortices as shown in Figure 3. The solutions originate from a saddle-node bifurcation at a finite value of the Reynolds number. The one with threefold rotational symmetry appears at the lowest onset Reynolds number (Wedin & Kerswell 2004), although it was later found that travelling waves without any discrete rotational symmetry exist at much lower Reynolds numbers (Pringle & Kerswell 2007).

As in circular pipes, the laminar flow in a square duct is linearly stable, and no

travelling-wave solutions were known until three such solutions were found using the homotopy approach, introducing either an artificial body force or internal heating. Two of them found by Okino et al. (2010), Wedin et al. (2009) have streaks and streamwise vortices on only two opposite walls, while the flow near the other two walls of the duct is quiescent. The other travelling wave obtained by Uhlmann et al. (2010), on the other hand, features streaks and vortices in the vicinity of all four walls, as will be discussed in Section 4.3 (see Figure 8).

Most of above-mentioned equilibrium solutions for plane channels, circular pipes and square ducts look qualitatively similar in spite of differences in their geometry and driving mechanisms (Kawahara et al. 2003, Waleffe 1998). Their structure is characterized by a wavy low-velocity streak flanked by staggered quasi-streamwise vortices of alternating signs, resembling the spatially-coherent objects found in the near-wall region of true turbulent flows (see, e.g. Jeong et al. 1997, Stretch 1990).

### 3.2 Periodic Solutions

We have just seen that three-dimensional equilibrium solutions reproducing buffer-layer coherent structures are available for a variety of wall-bounded flows. A smaller number of periodic solutions have been reported.

In plane Couette flow, Clever & Busse (1997) analysed the linear stability of the three-dimensional steady solution of Nagata (1990), and they identified a Hopf bifurcation from which a three-dimensional, nonlinear periodic solution originates. They continued that solution within its stable parameter range by forward time integration, but found that its properties did not differ too much from those of the steady solution due to the small amplitude of the oscillations. Using an iterative method, Kawahara & Kida (2001) found a more unsteady three-dimensional unstable periodic solution, which reproduces much better the full regeneration cycle of near-wall streamwise vortices and low-velocity streaks, as will be shown in Section 4.1. They also obtained a gentler periodic solution that represents weak spanwise standing-wave motion of the low-velocity streak. More recently Viswanath (2007) used globally convergent Newton–Krylov iteration (see SIDEBAR) to obtain five new three-dimensional periodic solutions that demonstrate the breakup and reorganization of near-wall coherent structures.

In plane Poiseuille flow, Toh & Itano (2003) identified a three-dimensional periodic-like solution that could originate from a heteroclinic connection between two steady travelling waves that differ from each other by a spanwise shift of half a wavelength (Itano & Toh 2001). Their solution is reminiscent of the heteroclinic cycle identified in a highly reduced dynamical systems approximation to near-wall turbulence by Aubry et al. (1988), who also observed a connection between two equilibria differing by a similar spanwise shift.

More recently, Duguet et al. (2008) found a three-dimensional periodic solution in Hagen–Poiseuille flow that bifurcates from the travelling wave without any discrete rotational symmetry found by Pringle & Kerswell (2007).

Most unstable periodic solutions have been found for wall bounded shear flows, but there are a few exceptions. One is the periodic solution found by van Veen et al. (2006) in Kida–Pelz high-symmetric flow in a triply-periodic domain (Kida 1985), which reproduces the Kolmogorov (1941) universal energy spectrum with the correct energy dissipation rate as will be shown in Section 4.2, even though its Reynolds number is too low to identify any significant inertial range. The



inertial-range energy spectrum has not been found in any periodic solution to the Navier–Stokes equation yet; however, it as well as intermittency were observed in periodic solutions to the GOY (Gledzer–Ohkitani–Yamada) shell model (Kato & Yamada 2003).

### 3.3 Comparison of Solutions

As reviewed above, equilibrium and periodic solutions reproduce buffer-layer coherent structures in near-wall turbulence at least qualitatively. The characteristics of those solutions are now quantitatively compared in Figure 4, which has been adapted from Jiménez et al. (2005) by adding some of the solutions that have been found since then. Each solution is represented by a single point whose coordinates are the maximum values of the streamwise and wall-normal velocity fluctuation,  $u'_{max}$  and  $v'_{max}$ , of its intensity profiles. The streamwise and wall-normal velocity fluctuations have been taken as representing the intensities of the streamwise velocity streaks and of the quasi-streamwise vortices, respectively. Despite differences in their boundary conditions most solutions can be seen to fall into one of two classes: a “vortex-dominated” family, characterized by smaller  $u'_{max}$  and larger  $v'_{max}$ , and a “streak-dominated” one, characterized by larger  $u'_{max}$  and smaller  $v'_{max}$ .

In the upper-left corner of Figure 4 we find the vortex-dominated solutions, and in the lower-right corner the streak-dominated ones. The former are represented by Nagata (1990) upper-branch steady solutions and the Kawahara & Kida (2001) dynamic periodic solution for Couette flow, by Jiménez & Simens (2001) autonomous travelling waves and the Waleffe (2003) upper-branch travelling wave for Poiseuille flow, and by Kerswell (2005), Kerswell & Tutty (2007), Wedin & Kerswell (2004) fourfold rotationally symmetric travelling waves in pipe flow. Viswanath (2007) periodic solutions in plane Couette flow are also part of this family. The vortex-dominated invariant solutions are able to reproduce the velocity fluctuations comparable with near-wall turbulence.

The streak-dominated family includes Nagata (1990) lower-branch steady solutions and the Kawahara & Kida (2001) gentle periodic solution for Couette flow, and the Waleffe (2003) lower-branch travelling wave for Poiseuille flow, which, however, is too close to the saddle-node bifurcation to differ significantly from the corresponding upper branch. The steady travelling wave obtained by Itano & Toh (2001) and the heteroclinic connection identified by Toh & Itano (2003) in Poiseuille flow are also in the streak-dominated family. The streak-dominated solution is probably not directly related to turbulence, and it is now believed to play an important role in the subcritical transition to turbulence (see Eckhardt et al. 2008, 2007, Kerswell 2005). At subcritical Reynolds numbers some of the streak-dominated solutions for plane Poiseuille and Couette flow have only one unstable direction in phase space, so that those invariant sets and their stable manifolds form the laminar-turbulent separatrix (Itano & Toh 2001, Kawahara 2005, Schneider et al. 2008, Waleffe 2003, Wang et al. 2007).

Although closer to the streak-dominated family, the twofold rotationally symmetric travelling waves in pipe flow found by Kerswell (2005), Kerswell & Tutty (2007), Wedin & Kerswell (2004) seem to be in between the two families.

The upper-branch of the eight-vortex travelling wave in a square duct found by Uhlmann et al. (2010) has weak velocity fluctuations, but is relatively close to the vortex-dominated solutions. The corresponding lower-branch solution (not

shown), on the other hand, has a weaker  $u'_{max}$  than the upper-branch one, and is thus quite different from the streak-dominated solutions. However, such weak fluctuations in a square duct are believed to be a consequence of averaging only in the streamwise direction.

## 4 SIGNIFICANCE OF INVARIANT SOLUTIONS

In this section we shall discuss the possible relevance of the simple invariant solutions to turbulent flows. All the solutions described above are unstable at the Reynolds numbers at which turbulence is observed, but the dimensions of their unstable manifolds in phase space are typically low (see Kawahara 2005, Kawahara et al. 2006, Kerswell & Tutty 2007, van Veen et al. 2006, Viswanath 2009, Waleffe 2001, Wang et al. 2007). Therefore, although we should not expect to observe them as such in real turbulence, a generic turbulent solution could approach them and spend a substantial fraction of its lifetime in their neighbourhood. Each of the invariant solutions has stable and unstable manifolds, and their intersections contain connecting orbits for the state of the system to follow as it visits these building blocks, associated with coherent structures. Some of these connecting orbits are associated with chaotic dynamics described mathematically by Smale's horseshoe map (Wiggins 1990). Such structures are called homoclinic and heteroclinic tangles. Hence, stable and unstable manifolds of the above simple invariant solutions could represent turbulence dynamics, while the simple solutions themselves would represent coherent structures embedded in a turbulent state.

### 4.1 Near-Wall Regeneration Cycle

In the buffer region of wall turbulence it is known that there exist self-sustaining coherent structures, namely quasi-streamwise vortices and low-velocity streaks, which control the near-wall flow dynamics. Low-velocity streaks have been recognized to be generated by cross-streamwise advection of vorticity lines of mean shear flow by streamwise vortices (Kline et al. 1967), and it is believed that the streamwise vortices arise from the instability of the streak and the subsequent nonlinear vortex stretching in the streamwise direction (Hamilton et al. 1995, Kawahara et al. 2003, Schoppa & Hussain 2002). These mutual generation processes are thought to form a closed nonlinear regeneration cycle of the streaks and the vortices (Hamilton et al. 1995, Waleffe 1997). Such a nonlinear cycle (in other words, self-sustaining process) of buffer-layer coherent structures has been described theoretically in terms of equilibrium or temporally periodic solutions to the incompressible Navier–Stokes equation for plane channel flows.

In order to relate a nonlinear equilibrium state with the self-sustaining process of buffer-layer coherent structures Waleffe (2001, 2003) introduced a spanwise periodic array of streamwise-independent rolls as external forcing to the Navier–Stokes equation. In this forced system there is a steady state that is represented by the low- and high-velocity streaks formed under the action of the imposed streamwise vortices. This basic steady state, composed of streaks, can lose its stability to a sinuous disturbance beyond some critical value of the roll strength, i.e. the amplitude of the external forcing. The nonlinear three-dimensional steady (travelling-wave) solutions, i.e. Nagata's solution in plane Couette flow and Waleffe's solution in plane Poiseuille flow (Nagata 1990, Waleffe 2001, 2003), bifurcate

from the basic state subcritically, yielding the zero-forcing state which is a solution to the Navier–Stokes equation. Such nonlinear solutions can be considered to represent the self-sustaining process in the sense that they appear from the formation of the streaks by the vortices and the generation of the vortices through the streak instability.

The nonlinear equilibrium solutions are considered to be the simplest description of the self-sustaining process of near-wall coherent structures. In order to describe the dynamics of their regeneration cycle, however, we should obtain more complex solutions. One candidate of such solutions is the vortex-dominated periodic solution found by Kawahara & Kida (2001) for plane Couette flow. A full cycle of the temporal evolution of spatial structures of this periodic solution is depicted in Figure 5 (*a–c*). Spatial structures of a turbulent solution are also shown at corresponding phases. The friction Reynolds number of the periodic solution is  $Re_\tau = 34$ , and the time period is  $65h/U (= 188\nu/u_\tau^2)$ . The streamwise and spanwise computational periods are  $L_x^+ \times L_z^+ = 188 \times 128$ . The dynamics of the periodic solution is described by a cyclic sequence of events which consists of

- (i) Figure 5 (*a*): the formation of low-velocity streaks through the cross-streamwise advection of streamwise velocity induced by decaying streamwise vortices;
- (ii) Figure 5 (*b*): the development of the streaks, and their subsequent sinuous bending along the streamwise direction as well as tilting in the spanwise ( $z$ ) direction; and
- (iii) Figure 5 (*c*): the regeneration of streamwise vortices as the consequence of the above streak instability in Figure 5 (*b*).

This cyclic sequence is completely consistent with a previously reported regeneration cycle (Hamilton et al. 1995, Waleffe 1997), and the wavy low-velocity streak and staggered counter-rotating streamwise vortices at phase (*b*) are closely similar to the coherent structures commonly observed in the buffer layer turbulence (Jeong et al. 1997, Stretch 1990).

## 4.2 Turbulence Statistics for the Viscous Range

There are two types of canonical turbulent flows, one of which is wall turbulence and the other of which is isotropic turbulence. In the near-wall region of any turbulent flow, which is referred to as the inner layer, the mean velocity is observed to scale with the kinematic viscosity  $\nu$  and the wall friction velocity  $u_\tau$  (Prandtl 1932). This is known as the Prandtl wall law, and one of the most typical universal statistical laws of fluid turbulence. It is also expected that statistical properties of small-scale turbulence in any flow away from a wall are nearly isotropic as a consequence of a nonlinear energy cascade process. The energy spectrum of small-scale motion in such flows is known to scale with  $\nu$  and the mean energy dissipation rate per unit mass  $\epsilon$  (Kolmogorov 1941). This is what we call the Kolmogorov similarity law, another universal law of turbulence. Here we discuss the relevance of the invariant solutions to turbulence statistics.

Figure 6 compares the normalised mean velocity profile for the Kawahara & Kida (2001) time-periodic solutions in plane Couette flow with those for turbulent flow. Open red symbols denote the vortex-dominated periodic solution ( $Re_\tau = 34$ ; see the large red loop in Figure 4) representing the regeneration cycle, while

closed blue symbols indicate the streak-dominated periodic solution with a gentle variation ( $Re_\tau = 28$ ; see the small blue loop in Figure 4). The mean velocity for the vortex-dominated periodic solution is in excellent agreement with that for the turbulent solutions not only at  $Re_\tau = 34$  but also at  $Re_\tau = 590$  (Moser et al. 1999) within the buffer layer, say at  $y^+ \lesssim 20$ , while that for the streak-dominated solution is closer to the laminar velocity profile. Although the logarithmic velocity profile in the overlap region cannot be seen in the vortex-dominated solution at the low Reynolds number  $Re_\tau = 34$ , this solution reproduces Prandtl's scaling law with  $\nu$  and  $u_\tau$  in the viscous wall layer.

In Figure 7, the normalised energy spectrum for a periodic orbit obtained by van Veen et al. (2006) in Kida–Pelz flow (Kida 1985) at the Taylor-microscale Reynolds number  $Re_\lambda = 67$  is shown, along with the spectrum for the turbulent solution. The time period of the solution is  $58(\nu/\epsilon)^{1/2}$ . The spectra for the periodic and turbulent solutions are in excellent agreement, and they are consistent with the turbulence spectra obtained by experiments (Champagne et al. 1970) and by closure theory (Kida & Goto 1997) in the high-wavenumber range, implying that the periodic solution represents the Kolmogorov dissipation-range energy spectrum. Actually, it has been confirmed that around  $Re_\lambda = 67$  the energy dissipation rate  $\epsilon$  for the periodic solution is nearly independent of  $\nu$  and takes almost the same value as that of turbulence. This result also implies that the energy spectrum for the periodic solution scales with  $\nu$  and  $\epsilon$  as for the turbulent state. As shown in Figure 7, however, the Reynolds number, at which the periodic solution has been obtained, is not high enough to clearly show the  $-5/3$  power spectrum for the inertial range observed both in the experiments and the theory.

It is curious that averaging along a single periodic solution of a relatively short period for plane Couette flow (Kawahara & Kida 2001) and Kida–Pelz flow (van Veen et al. 2006), reproduces so well typical turbulence statistics for the viscous range, such as the mean velocity profile in the buffer layer and the dissipation-range energy spectrum, which are long-time averages along true turbulent orbits.

One interesting idea was proposed by Kawasaki & Sasa (2005). They conjectured that relatively short periodic solutions give good statistics for quantities such as the energy dissipation rate because these are averages over the spatial domain. In a relatively large spatial domain, many quasi-independent processes of flow dynamics will occur simultaneously and thus averaging over space is not unlike averaging over time.

Saiki & Yamada (2010) studied periodic solutions to the Kuramoto–Sivashinsky equation. They compared time-mean values along the periodic solutions to those along chaotic segments of equal length, and found that the former are more narrowly distributed around the same average. This observation suggests that a good representation of flow statistics might be a generic property of relatively short periodic solutions embedded in spatio-temporal chaos.

### 4.3 Mean Secondary Flow

Turbulent flow through straight pipes with non-circular cross-section exhibits a mean secondary flow in the cross-sectional plane, whereas laminar flow does not. A satisfactory description of the mechanism leading to the formation of such secondary flow of Prandtl's second kind has been an outstanding issue for many decades, despite continuous efforts from a number of researchers. In the

following we will focus our attention on one geometry, namely the flow through a square duct. Recent vortex eduction studies based on DNS data have shown that the mean secondary flow can be linked to a non-homogeneous probability distribution of coherent flow structures along the duct perimeter (Pinelli et al. 2010, Uhlmann et al. 2007). In a statistical sense, mean secondary flow vorticity can be understood as a footprint of the preferential spatial occurrence of streamwise vortices caused by the cross-sectional geometry. These DNS studies have also revealed a succession of the most probable instantaneous streak-vortex patterns when increasing the Reynolds number from a value just above the limit for sustained turbulence ( $Re \equiv Uh/\nu = 1100$ ,  $U$  being the average mean velocity and  $h$  the duct half-width) to moderate values ( $Re = 3500$ ). At the lowest Reynolds numbers, the near-wall regeneration cycle is often simultaneously active at only two opposite walls (both featuring a single low-velocity streak and corresponding streamwise vortices), while the flow near the other pair of walls is quiescent (regime I). Above  $Re \approx 1400$ , the most probable state is characterized by simultaneous turbulence activity (a single streak associated with vortices) on all four walls (regime II). When further increasing the Reynolds number above  $Re \approx 2000$ , the most probable number of low-velocity streaks per wall increases to two (regime III). Further transitions have not been described in detail, due to the limited range of Reynolds numbers accessible to DNS. The statistical mean flow, on the other hand, always features the same number of two secondary flow vortices per wall (i.e. a total of eight per cross-section), with a given sense of rotation, albeit with changing shape as a function of the Reynolds number.

Among the presently known travelling waves, the solutions of Okino et al. (2010) and Uhlmann et al. (2010) have the potential to represent coherent structures in turbulent duct flow in different respective Reynolds number ranges. The former solution exhibits coherent structures which appear to be consistent with observations in turbulent flow pertaining to regime I, while the latter solution matches some of the characteristics related with coherent structures found in regime II as well as the mean secondary flow in both regimes II and III, as will be discussed next.

Focusing on the solution by Uhlmann et al. (2010), Figure 8 shows the flow field on the upper branch at  $Re = 1404$ . It can be seen that a wavy low-speed streak as well as staggered streamwise vortices are found in the vicinity of all four wall planes, as observed in turbulent flow in regime II. Furthermore, the streamwise average of this solution exhibits a secondary flow pattern with eight vortices, strikingly resembling the statistically averaged secondary flow observed in turbulence at the same Reynolds number (Uhlmann et al. 2010). The comparison of this travelling wave solution with turbulence data is further elaborated in Figure 9, where the secondary flow intensity is shown as a function of the bulk Reynolds number. At low Reynolds numbers (pertaining to regime I) the upper branch solution of Uhlmann et al. (2010) by far exceeds intensity levels found in turbulent flow; beyond  $Re \approx 1400$  (i.e. in regimes II and III), however, both quantities are comparable, implying that the upper branch could represent mean secondary flow at any value of higher Reynolds number. In contrast with the secondary flow the perturbation energy as well as the friction factor (not shown) are found to match statistical data from turbulence in a narrow range of Reynolds numbers corresponding to regime II.

In conclusion, we state that it is significant for simple invariant solutions to represent not only spatio-temporal coherence in turbulent flows but also typical

statistical properties of turbulence.

## 5 FUTURE DIRECTIONS

Finally, we briefly discuss possible future areas of research in this nascent field of the relation of the coherent structures and turbulence statistics to dynamical systems. Although it has turned out that the structures, the dynamics, and the statistics of buffer-layer coherent structures are tantalizingly close to those of some nonlinear equilibria or periodic solutions, the dynamical interpretation of the large-amplitude intermittent events observed in the near-wall region is still unclear. The invariant solutions computed so far are not very useful for explaining intermittent behaviour in turbulence because they lack localization. They have been computed in small, periodic, domains and persist for all time.

In order to describe the intermittency we will need to compute solutions which display localization in the spatial domain, the temporal domain or both. Good candidates for localized solutions are homoclinic and heteroclinic orbits. In the temporal domain, i.e. in the sense of Section 2.2, such solutions correspond to large excursions in phase space while transiting between simple invariant solutions. In the spatial domain, such solutions correspond to different phases of the flow coexisting in physical space, glued together by sharp interfaces. Computation of orbits connecting invariant sets in time is hard because they need to be approximated over long time intervals. The sensitive dependence on initial conditions makes this computation potentially unstable, as any kind of numerical noise is amplified during time-stepping.

An attempt to explain bursting, i.e. temporal intermittency, through connecting orbits was made recently by van Veen & Kawahara (2011). They studied the gentle periodic solution identified by Kawahara & Kida (2001). This periodic solution has a single unstable multiplier and its stable manifold separates the phase space into two parts, one containing the domain of attraction of the laminar flow (Kawahara 2005). A piece of the two-dimensional unstable manifold can be computed by Newton–Krylov continuation of orbit segments. A boundary value problem is set up which specifies that the initial point of the segment must lie in the linear approximation of the manifold, whereas the final point satisfies some scalar condition, e.g. the energy dissipation rate has a fixed value. This boundary value problem is under-determined by a single degree of freedom and thus we can compute a family of orbit segments by arclength continuation (van Veen et al. 2011). Since a connecting orbit separates the manifold into two components, the consecutive orbits segments can converge to a connecting orbit during the continuation. In Figure 10 an orbit homoclinic to the gentle periodic solution is shown, which makes a large excursion during which the energy dissipation rate reaches more than twice the mean value in periodic motion and four times the value at the laminar equilibrium. In the dissipative phase of this bursting cycle, as shown in Figure 11, at the valley and the crest of the streaks small quasi-streamwise vortices are formed and move rapidly in the spanwise direction, and the larger part of the energy dissipation takes place there. Similar dissipative flow structures are also observed during bursting in a turbulent state, and they are very different from those for the vortex-dominated periodic solution, in other words the regeneration cycle, in Figure 5.

For now only a few spatially localized invariant solutions are available. Such

solutions were first computed in plane Couette flow by Cherhabili & Ehrenstein (1997) and revisited by Ehrenstein et al. (2008). They found three-dimensional equilibrium states which are localized in the streamwise direction. Schneider et al. (2010) studied the same flow at lower Reynolds numbers, but focused on the dependence of certain equilibria and traveling waves on the spanwise extent of the computational domain. They found that for domain sizes substantially larger than the minimal flow unit, some of these equilibria become localized in the spanwise direction. Towards the edges of the spanwise domain, the flow is laminar but in the centre there are a number of streamwise vortices. The creation of vortex pairs takes place at saddle-node bifurcations in an intricate diagram called a homoclinic snake. Further search for localized invariant solutions should lead to understanding of typical spatially-intermittent turbulence, such as turbulent spots (Dauchot & Daviaud 1995), oblique stripes (Prigent et al. 2002) and puffs (Wynanski & Champagne 1973).

Another important problem to be tackled is the relevance of simple invariant solutions to high-Reynolds-number turbulent flows. As reviewed in this paper, essential dynamics of buffer-layer structures has been described in terms of invariant solutions. They can also reproduce the mean velocity profile in the near-wall layer of turbulent flow and the energy spectrum in the dissipation range of isotropic turbulence. However, we have no simple invariant solutions which reproduce the universal statistical laws of turbulence, i.e. the logarithmic velocity profile or the  $-5/3$ -power energy spectrum in high-Reynolds-number turbulence. If such solutions exist, there would be an interesting question as to whether or not they could represent larger-scale structures and their dynamics in the logarithmic layer (see Jiménez 2011) and in the inertial range. Flores & Jiménez (2010) have recently found quasi-periodic bursts in the logarithmic region of fully turbulent channel flow, strongly reminiscent of the regeneration cycle in the buffer layer, suggesting that the large-scale dynamics in the logarithmic layer might be related to invariant solutions in larger periodic domains at high Reynolds number. This problem is quite challenging to a dynamical systems approach to turbulent flows as well as to large-scale scientific computations.

## SUMMARY POINTS

1. An overview of a dynamical systems approach to turbulence has been presented, based on recently found simple invariant solutions and connecting orbits in Navier-Stokes flow.
2. In wall-bounded shear flows, these solutions come in two families: vortex-dominated and streak-dominated. The former family reproduces buffer-layer coherent structures and velocity fluctuations comparable to near-wall turbulence, while the latter appears to regulate transition to turbulence in the presence of a stable laminar flow.
3. Vortex-dominated periodic solutions in plane Couette flow have been shown to reproduce the regeneration cycle of the coherent structures and Prandtl's wall law in the viscous wall layer, while periodic solutions in Kida-Pelz flow have been found with a Kolmogorov spectrum in the dissipation range.
4. In the square duct, travelling-wave solutions have been found which lead to consistent patterns and intensities as compared to turbulence-driven mean secondary flow.

5. In plane Couette flow, equilibria and travelling waves have been computed which exhibit localization either in the spanwise or the streamwise direction. Also, a connecting orbit has been computed which shows turbulent bursting localized in time. Such solutions reproduce the intermittent nature of transitional flows.

## FUTURE ISSUES

1. Can we obtain spatially-localized invariant solutions to reproduce spatial intermittency of turbulence, such as turbulent spots, puffs and stripes observed in large domains?
2. Can we find periodic solutions in sufficiently large domains and at sufficiently large Reynolds number to reproduce the logarithmic law for wall bounded flows and Kolmogorov's inertial-range scaling for isotropic turbulence?
3. Can we compute a sufficient number of invariant solutions for a given flow to be fully decomposed into building blocks, i.e. simple invariant solutions (coherent structures) and their connecting orbits (turbulence dynamics)?

## ACKNOWLEDGMENTS

The authors cordially thank Prof. F. Waleffe, Prof. R. Kerswell and Prof. D. Viswanath for their original figures and data for Figures 2, 3 and 4. Several of the results presented in Sections 3 and 4 are outcomes from the authors' collaboration with Prof. S. Kida, Prof. J. Jiménez, Prof. M. Nagata and Dr. A. Pinelli. The authors greatly appreciate their discussions in the course of the collaboration. G.K. is supported by a Grant-in-Aid for Scientific Research (B) from the Japanese Society for the Promotion of Science. L.v.V. is supported by NSERC Grant nr. 355849-2008.

## References

- Artuso R, Aurell E, Cvitanović P. 1990a. Recycling of strange sets: I. Cycle expansions. *Nonlinearity* 3:325–359
- Artuso R, Aurell E, Cvitanović P. 1990b. Recycling of strange sets: II. Applications. *Nonlinearity* 3:361–386
- Aubry N, Holmes P, Lumley JL, Stone E. 1988. The dynamics of coherent structures in the wall region of a turbulent boundary layer. *J. Fluid Mech.* 192:115–173
- Champagne FH, Harris VG, Corrsin S. 1970. Experiments on nearly homogeneous turbulent shear flow. *J. Fluid Mech.* 41:81–139
- Cherhabili A, Ehrenstein U. 1997. Finite-amplitude equilibrium states in plane Couette flow. *J. Fluid Mech.* 342:159–177
- Christiansen F, Cvitanović P, Putkaradze V. 1997. Spatiotemporal chaos in terms of unstable recurrent patterns. *Nonlinearity* 10:55–70
- Clever RM, Busse FH. 1992. Three-dimensional convection in a horizontal fluid layer subjected to a constant shear. *J. Fluid Mech.* 234:511–527



- Clever RM, Busse FH. 1997. Tertiary and quaternary solutions for plane Couette flow. *J. Fluid Mech.* 344:137–153
- Cvitanović. 1987. Invariant measurement of strange sets in terms of cycles. *Phys. Rev. Lett.* 61:2729–2732
- Cvitanović P, Artuso R, Mainieri R, Tanner G, Vattay G. 2010. *Chaos: Classical and Quantum*. ChaosBook.org/version13 (Niels Bohr Institute, Copenhagen)
- Dauchot O, Daviaud F. 1995. Finite amplitude perturbation and spots growth mechanism in plane Couette flow. *Phys. Fluids* 7:335–343
- Dennis JE, Schnabel RB. 1996. *Numerical Methods for Unconstrained Optimization and Nonlinear Equations*, vol. 16 of *Classics in applied mathematics*. SIAM
- Dickson KI, Kelley CT, Ipsen ICF, Kevrekidis IG. 2007. Condition estimates for pseudo-arclength continuation. *SIAM J. Numer. Anal.* 45:263–276
- Duguet Y, Pringle CC, Kerswell RR. 2008. Relative periodic orbits in transitional pipe flow. *Phys. Fluids* 20:114102
- Eckhardt B, Faisst H, Schmiegél A, Scheider TM. 2008. Dynamical systems and the transition to turbulence in linearly stable shear flows. *Phil. Trans. R. Soc. A* 366:1297–1315
- Eckhardt B, Scheider TM, Hof B, Westerweel J. 2007. Turbulence transition in pipe flow. *Ann. Rev. Fluid Mech.* 39:447–468
- Ehrenstein U, Koch W. 1991. Three-dimensional wavelike equilibrium states in plane Poiseuille flow. *J. Fluid Mech.* 228:111–148
- Ehrenstein U, Nagata M, Rincon F. 2008. Two-dimensional nonlinear plane Poiseuille–Couette flow homotopy revisited. *Phys. Fluids* 20:064103
- Faisst H, Eckhardt B. 2003. Traveling waves in pipe flow. *Phys. Rev. Lett.* 91:224502
- Fazendeiro L, Boghosian BM, Coveney PV, Lätt J. 2010. Unstable periodic orbits in weak turbulence. *J. Comput. Sci.* 1:13–23
- Flores O, Jiménez J. 2010. Hierarchy of minimal flow units in the logarithmic layer. *Phys. Fluids* 22:071704
- Foias C, Manley O, Rosa R, Temam R. 2001. *Navier–Stokes Equations and Turbulence*. Cambridge Univ. Press, 1st ed.
- Gibson JF. 2007. Channelflow: a spectral navier-stokes simulator in C++. Tech. Rep., Georgia Institute of Technology. Available from [www.channelflow.org](http://www.channelflow.org)
- Gibson JF, Halcrow J, Cvitanović P. 2008. Visualizing the geometry of state space in plane Couette flow. *J. Fluid Mech.* 611:107–130
- Gibson JF, Halcrow J, Cvitanović P. 2009. Equilibrium and travelling-wave solutions of plane Couette flow. *J. Fluid Mech.* 638:243–266
- Hamilton JM, Kim J, Waleffe F. 1995. Regeneration mechanisms of near-wall turbulence structures. *J. Fluid Mech.* 287:317–348
- Holmes P, Lumley JL, Berkooz G. 1996. *Turbulence, Coherent Structures, Dynamical Systems and Symmetry*. Cambridge Univ. Press, 1st ed.
- Itano T, Generalis SC. 2009. Hairpin vortex solution in planar Couette flow: A tapestry of knotted vortices. *Phys. Rev. Lett.* 102:114501

- Itano T, Toh S. 2001. The dynamics of bursting process in wall turbulence. *J. Phys. Soc. Jpn.* 70:703–716
- Jeong J, Hussain F, Schoppa W, Kim J. 1997. Coherent structures near the wall in a turbulent channel flow. *J. Fluid Mech.* 332:185–214
- Jiménez J. 1987. Coherent structures and dynamical systems. In *Proc. CTR Summer Program 1987*. Stanford Univ.
- Jiménez J. 2011. Multi-scale dynamics in wall-bounded turbulence. *Ann. Rev. Fluid Mech.* 44
- Jiménez J, Kawahara G. 2011. Dynamics of wall-bounded turbulence. In *Preprint*. Cambridge Univ. Press
- Jiménez J, Kawahara G, Simens MP, Nagata M, Shiba M. 2005. Characterization of near-wall turbulence in terms of equilibrium and ‘bursting’ solutions. *Phys. Fluids* 17:015105
- Jiménez J, Moin P. 1991. The minimal flow unit in near-wall turbulence. *J. Fluid Mech.* 225:221–240
- Jiménez J, Pinelli A. 1999. The autonomous cycle of near wall turbulence. *J. Fluid Mech.* 389:335–359
- Jiménez J, Simens MP. 2001. Low-dimensional dynamics in a turbulent wall flow. *J. Fluid Mech.* 435:81–91
- Kato S, Yamada M. 2003. Unstable periodic solutions embedded in a shell model turbulence. *Phys. Rev. E* 68:025302(R)
- Kawahara G. 2005. Laminarization of minimal plane Couette flow: Going beyond the basin of attraction of turbulence. *Phys. Fluids* 17:041702
- Kawahara G, Jiménez J, Uhlmann M, Pinelli A. 2003. Linear instability of a corrugated vortex sheet – a model for streak instability. *J. Fluid Mech.* 483:315–342
- Kawahara G, Kida S. 2001. Periodic motion embedded in plane Couette turbulence: regeneration cycle and burst. *J. Fluid Mech.* 449:291–300
- Kawahara G, Kida S, Nagata M. 2006. Unstable periodic motion in plane Couette system: the skeleton of turbulence. In *IUTAM symposium on one hundred years of boundary layer research*. Springer
- Kawasaki M, Sasa Si. 2005. Statistics of unstable periodic orbits of a chaotic dynamical system with a large number of degrees of freedom. *Phys. Rev. E* 72:037202
- Keefe L, Moin P, Kim J. 1992. The dimension of attractors underlying periodic turbulent Poiseuille flow. *J. Fluid Mech.* 242:1–29
- Kerswell RR. 2005. Recent progress in understanding the transition to turbulence in a pipe. *Nonlinearity* 18:R17–R44
- Kerswell RR, Tutty OR. 2007. Recurrence of travelling waves in transitional pipe flow. *J. Fluid Mech.* 584:69–102
- Kida S. 1985. Three-dimensional periodic flows with high-symmetry. *J. Phys. Soc. Japan* 54:2132–2136
- Kida S, Goto S. 1997. A lagrangian direct-interaction approximation for homogeneous isotropic turbulence. *J. Fluid Mech.* 345:307–345

- Kim J, Moin P, Moser RD. 1987. Turbulence statistics in fully developed channel flow at low Reynolds number. *J. Fluid Mech.* 177:133–166
- Kline SJ, Reynolds WC, Schraub FA, Runstadler PW. 1967. The structure of turbulent boundary layers. *J. Fluid Mech.* 30:741–773
- Kolmogorov AN. 1941. The local structure of turbulence in incompressible viscous fluids at very large Reynolds numbers. *Dokl. Akad. Nauk. SSSR* 30:301–305. Reprinted in *Proc. R. Soc. London. A* **434**, 9–13 (1991)
- Lan Y, Cvitanović P. 2004. Variational method for finding periodic orbits in a general flow. *Phys. Rev. E* 69:016217
- Landau LD, Lifshitz EM. 1959. *Fluid Mechanics*. Pergamon Press, 1st ed.
- Moser RD, Kim J, Mansour NN. 1999. Direct numerical simulation of turbulent channel flow up to  $Re_\tau = 590$ . *Phys. Fluids* 11:943–945
- Nagata M. 1990. Three-dimensional finite-amplitude solutions in plane Couette flow: bifurcation from infinity. *J. Fluid Mech.* 217:519–527
- Nagata M. 1997. Three-dimensional traveling-wave solutions in plane Couette flow. *Phys. Rev. E* 55:2023–2025
- Okino S, Nagata M, Wedin H, Bottaro A. 2010. A new nonlinear vortex state in square-duct flow. *J. Fluid Mech.* 657:413–429
- Pinelli A, Uhlmann M, Sekimoto A, Kawahara G. 2010. Reynolds number dependence of mean flow structure in square duct turbulence. *J. Fluid Mech.* 644:107–122
- Prandtl L. 1932. Zur turbulenten strömung in rohren und längs platten. *Ergeb. AVA Göttingen* 4:18–29
- Prigent A, Grégoire G, Chaté H, Dauchot O, van Saarloos W. 2002. Large-scale finite-wavelength modulation within turbulent shear flows. *Phys. Rev. Lett.* 89:014501
- Pringle CC, Kerswell RR. 2007. Asymmetric, helical, and mirror-symmetric traveling waves in pipe flow. *Phys. Rev. Lett.* 99:074502
- Saad Y. 2003. *Iterative Methods for Sparse Linear Systems. Second Edition*. SIAM
- Saiki Y, Yamada M. 2010. Unstable periodic orbits embedded in a continuous time dynamical system – time averaged properties. *RIMS Kokyuroku* 1713:111–123
- Sánchez J, Net M, García-Archilla B, Simó C. 2004. Newton-Krylov continuation of periodic orbits for Navier-Stokes flows. *J. Comp. Phys.* 201:13–33
- Schmiegel A. 1999. *Transition to turbulence in linearly stable shear flows*. Ph.D. thesis, Faculty of Physics, Philipps-Universität Marburg
- Schneider TM, Gibson JF, Burke J. 2010. Snakes and ladders: localized solutions of plane Couette flow. *Phys. Rev. Lett.* 104:104501
- Schneider TM, Gibson JF, Lagha M, De Lillo F, Eckhardt B. 2008. Laminar-turbulent boundary in plane Couette flow. *Phys. Rev. E* 78:037301
- Schoppa W, Hussain F. 2002. Coherent structure generation in near-wall turbulence. *J. Fluid Mech.* 453:57–108

- Siminos E, Cvitanović P. 2011. Continuous symmetry reduction and return maps for high-dimensional flows. *Physica D* 240:187–198
- Stretch DD. 1990. Automated pattern eduction from turbulent flow diagnostics. In *CTR Ann. Res. Briefs*. Stanford Univ.
- Toh S, Itano T. 2003. A periodic-like solution in channel flow. *J. Fluid Mech.* 481:67–76
- Tuckerman L, Barkley D. 2000. *Numerical Methods for Bifurcation Problems and Large-Scale Dynamical Systems*, chap. Bifurcation analysis for timesteppers. IMA Volumes in Mathematics and its Applications. Springer, 453–466
- Uhlmann M, Kawahara G, Pinelli A. 2007. Marginally turbulent flow in a square duct. *J. Fluid Mech.* 588:153–162
- Uhlmann M, Kawahara G, Pinelli A. 2010. Traveling-waves consistent with turbulence-driven secondary flow in a square duct. *Phys. Fluid* 22:084102
- van Veen L, Kawahara G. 2011. A homoclinic tangle at the edge of shear turbulence. *submitted*
- van Veen L, Kawahara G, Matsumura A. 2011. On matrix-free computation of 2D unstable manifolds. *SIAM J. Sci. Comp.* 33:25–44
- van Veen L, Kida S, Kawahara G. 2006. Periodic motion representing isotropic turbulence. *Fluid Dynamics Research* 38:19–46
- Viswanath D. 2007. Recurrent motions within plane Couette turbulence. *J. Fluid Mech.* 580:339–358
- Viswanath D. 2009. The critical layer in pipe flow at high Reynolds number. *Phil. Trans. Roy. Soc. A* 367:561–576
- Waleffe F. 1997. On a self-sustaining process in shear flows. *Phys. Fluids* 9:883–900
- Waleffe F. 1998. Three-dimensional coherent states in plane shear flows. *Phys. Rev. Lett.* 81:4140–4143
- Waleffe F. 2001. Exact coherent structures in channel flow. *J. Fluid Mech.* 435:93–102
- Waleffe F. 2003. Homotopy of exact coherent structures in plane shear flows. *Phys. Fluids* 15:1517–1534
- Wang J, Gibson J, Waleffe F. 2007. Lower branch coherent states in shear flows: Transition and control. *Phys. Rev. Lett.* 98:204501
- Wedin H, Bottaro A, Nagata M. 2009. Three-dimensional traveling waves in a square duct. *Phys. Rev. E* 79:065305(R)
- Wedin H, Kerswell RR. 2004. Exact coherent structures in pipe flow: travelling wave solutions. *J. Fluid Mech.* 508:333–371
- Wiggins S. 1990. *Introduction to Applied Nonlinear Dynamical Systems and Chaos*. Springer
- Wynagnanski IJ, Champagne FH. 1973. On transition in a pipe. part 1. the origin of puffs and slugs and the flow in a turbulent slug. *J. Fluid Mech.* 59:281–335
- Yamada M. 2002. From laminar flow to turbulence (in Japanese). *Parity* 17:21–26

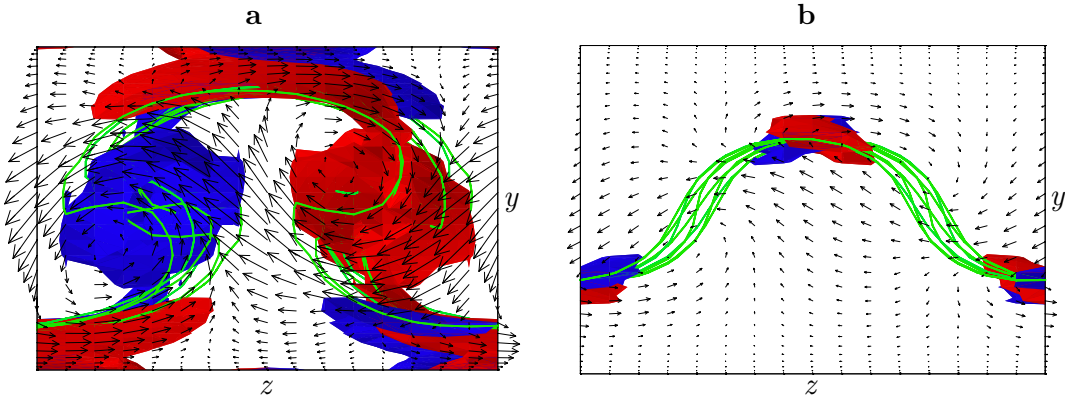


Figure 1: Projection of the streamwise ( $x$ ) vorticity  $\omega_x$  and velocity fields on the cross-stream plane  $(z, y)$  of the upper- and lower-branch Nagata (1990) solutions for plane Couette flow recomputed by Jiménez et al. (2005) at Reynolds number  $Re \equiv Uh/\nu = 400$ ,  $U$  and  $h$  being half the difference of the two wall velocities and half the wall separation, respectively. The streamwise and spanwise period for the solutions are  $L_x/h \times L_z/h = 2\pi \times 0.9\pi$ . The green lines are different sections of the surface of null streamwise velocity  $u = 0$ , i.e, the critical layer, and their corrugation represents a low-velocity streak. Arrows are the cross-plane velocities at  $x = 0$ . The red and blue objects are isosurfaces  $\omega_x^+ \equiv \omega_x \nu / u_\tau^2 = \pm 0.155$  representing streamwise vortices ( $u_\tau$  being the wall friction velocity). (a) upper branch,  $L_z^+ \equiv L_z u_\tau / \nu = 99$ ; (b) lower branch,  $L_z^+ = 67$ .

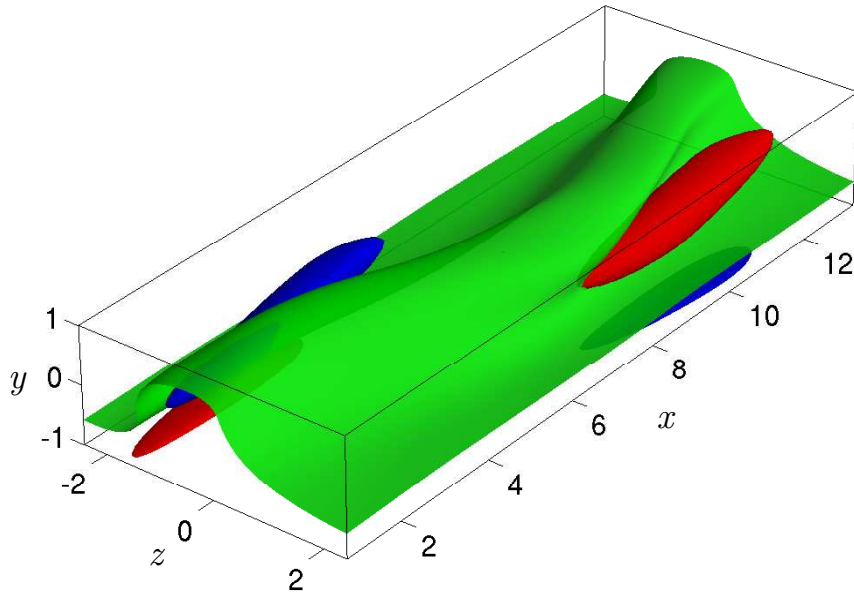


Figure 2: Steady travelling-wave solution for plane Poiseuille flow, computed by Waleffe (2001, 2003). The solution is shown at a saddle-node bifurcation at the lowest Reynolds number  $Re_\tau \equiv u_\tau h/\nu = 44$  with the optimal streamwise and spanwise periods  $L_x^+ \times L_z^+ = 274 \times 105$ . Streamwise vortices are visualized by the red and blue isosurfaces of the streamwise vorticity  $\omega_x = \pm 0.7 \max(\omega_x)$ . The corrugation of the green isosurface of the streamwise velocity  $u = 0.75 \max(u)$  represents a low-velocity streak. Flow is toward positive  $x$  and only half the height of the channel is shown.

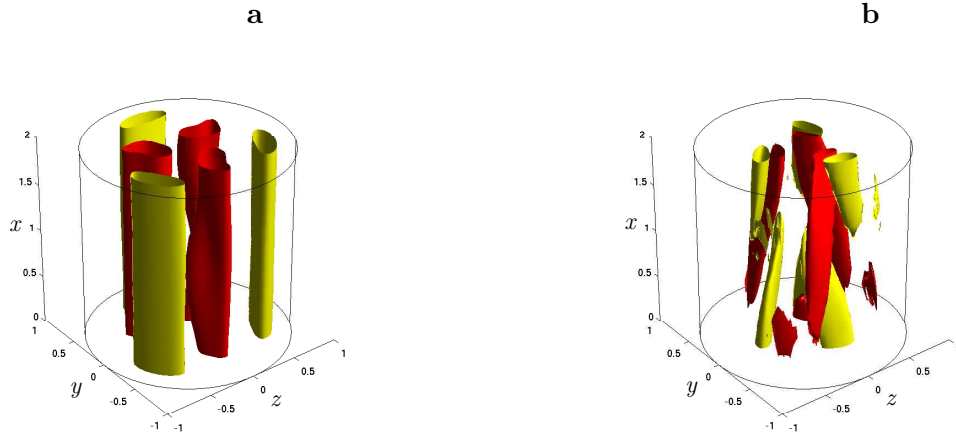


Figure 3: Perspective view of isosurfaces of (a) axial ( $x$ ) velocity fluctuation  $\pm 0.3U$  (yellow/red) from laminar Hagen–Poiseuille flow and (b) axial vorticity  $\omega_x = \pm 0.6U/D$  (yellow/red) for the threefold rotationally symmetric travelling-wave solution for pipe flow (Kerswell 2005, Kerswell & Tutty 2007, Wedin & Kerswell 2004) at Reynolds number  $Re \equiv UD/\nu = 2400$ ,  $U$  and  $D$  being bulk mean velocity and pipe diameter, respectively. The axial period for the solution is  $L_x/(D/2) = 2.01$ . Flow is upwards.

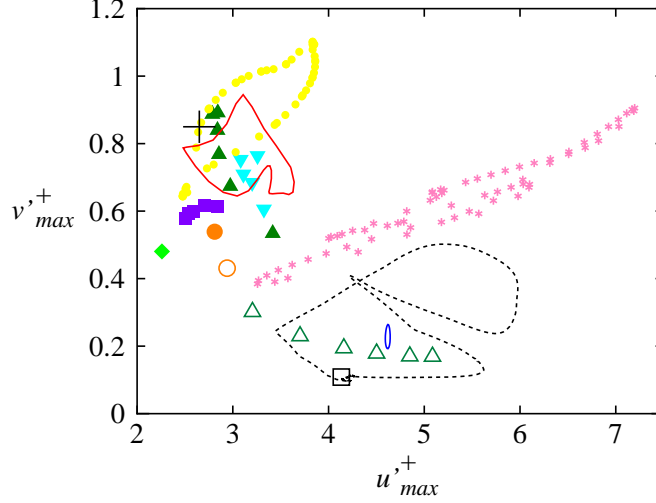


Figure 4: Classification into vortex- and streak-dominated families of the simple invariant solutions, in terms of their maximum streamwise and wall-normal r.m.s. velocities,  $u'_{max}$  and  $v'_{max}$  (Jiménez et al. 2005), normalised with the friction velocity  $u_\tau$ . Solid symbols are classified as vortex-dominated solutions, and open ones as streak-dominated solutions. The red and blue loops represent the dynamic ( $L_x^+ \times Re_\tau \times L_z^+ = 190 \times 34 \times 130$ ) and the gentle ( $L_x^+ \times Re_\tau \times L_z^+ = 154 \times 28 \times 105$ ) periodic solutions at  $Re = 400$  in Kawahara & Kida (2001).  $\triangle$ , Nagata steady solutions (Jiménez et al. 2005) for several values of the spanwise wavelength at  $Re = 400$  and  $L_x/h = 2\pi$  (upper branch,  $L_z^+ \times Re_\tau = 76 - 132 \times 35 - 35$ ; lower branch,  $L_z^+ \times Re_\tau = 53 - 92 \times 24 - 25$ ).  $\blacksquare$ , autonomous solutions in Jiménez & Simens (2001) ( $L_x^+ \times L_z^+ \times \delta^+ = 151 - 189 \times 180 \times 38 - 46$ , where  $\delta$  is the filter height).  $\circ$ , Waleffe (2003) travelling waves (upper branch,  $Q/\nu = 1303$ , where  $Q$  is the volume flux per unit span,  $L_x^+ \times Re_\tau \times L_z^+ = 387 \times 123 \times 149$ ; lower branch,  $Q/\nu = 1390$ ,  $L_x^+ \times Re_\tau \times L_z^+ = 379 \times 121 \times 146$ ).  $\square$ , Itano & Toh (2001) asymmetric wave for  $Q/\nu = 4000$ ,  $L_x/h \times L_z/h = \pi \times 0.4\pi$ . The dotted loop is the periodic-like solution of Toh & Itano (2003).  $\blacktriangledown$ , temporal averages of Viswanath (2007) periodic solutions (cases  $P_2 - P_6$  in his table 1) for  $Re = 400$  and  $L_x/h \times L_z/h = 1.75\pi \times 1.2\pi$ .  $\blacklozenge$ , upper branch of Uhlmann et al. (2010) eight-vortex travelling wave ( $Re = 1371$ ,  $L_x/h = 2\pi$ ).  $\bullet$ , Kerswell (2005), Kerswell & Tutty (2007), Wedin & Kerswell (2004) fourfold rotationally symmetric travelling waves for several values of the streamwise period at  $Re = 2000$  ( $\mathcal{R}_4$  travelling waves in figure 8 of Kerswell (2005)).  $*$ , twofold rotationally symmetric travelling waves (Kerswell 2005, Kerswell & Tutty 2007, Wedin & Kerswell 2004) for several values of the streamwise period at  $Re = 2000$  ( $\mathcal{R}_2$  travelling waves in figure 8 of Kerswell (2005)). We have also shown the turbulent state computed by Kim et al. (1987) ( $L_x^+ \times Re_\tau \times L_z^+ = 2300 \times 180 \times 1150$ ) by the symbol  $+$  for comparison.



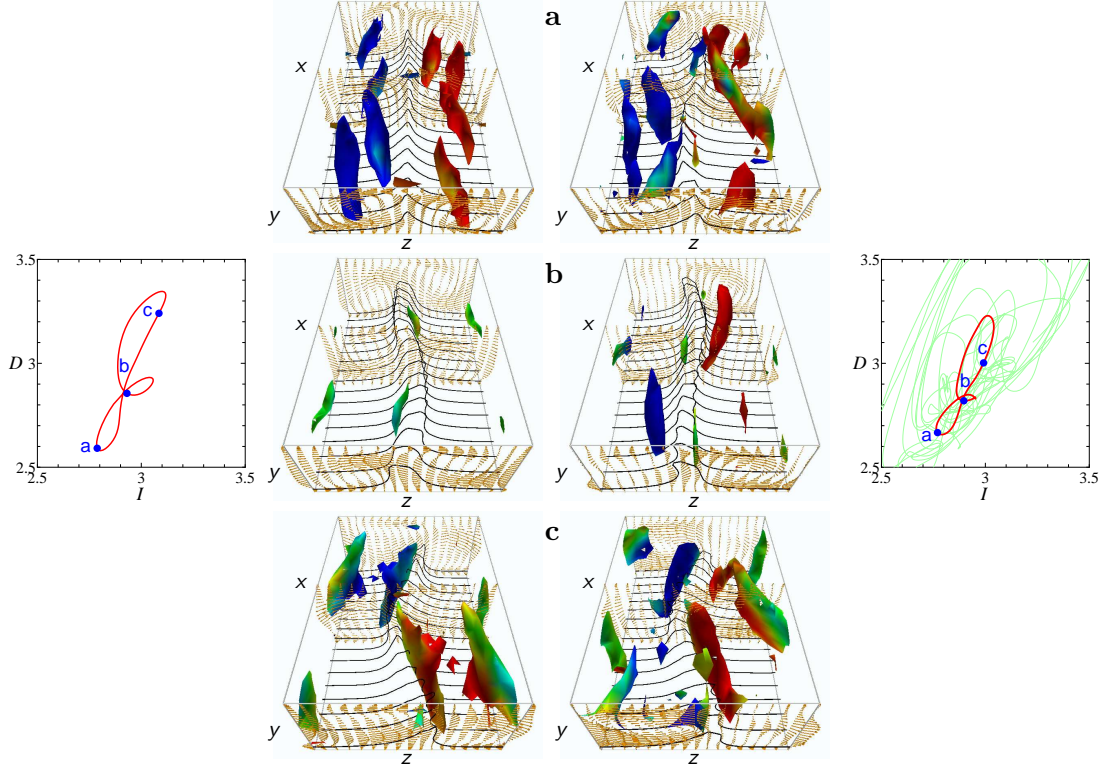


Figure 5: A cycle of evolution of spatial structures of the Kawahara & Kida (2001) vortex-dominated time-periodic solution (left) and those of the turbulent solution (right) at corresponding phases for plane Couette flow at  $Re = 400$ . Flow structures are visualized in the whole spatially periodic box ( $L_x \times 2h \times L_z$ ) over one full cycle at three times with a constant interval  $21.6h/U$ . The upper (or lower) wall moves into (or out of) the page at velocity  $U$  (or  $-U$ ). Vortex structures are represented by isosurfaces of the Laplacian of pressure,  $\nabla^2 p = 0.15\rho(U/h)^2$ , where  $\rho$  is the mass density of the fluid. Color of the isosurfaces of  $\nabla^2 p$  indicates the sign of the streamwise ( $x$ ) vorticity: red is positive (clockwise), blue is negative (counter-clockwise). Cross-flow velocity vectors and contours of the streamwise velocity at  $u = -0.3U$  are also shown on cross-flow planes  $x = \text{const}$ . The streamwise and spanwise period for the solution are  $L_x/h \times L_z/h = 1.755\pi \times 1.2\pi$ . The phases for the visualization are identified by the symbols **a**, **b**, **c** in the phase plane ( $I, D$ ) respectively for the periodic (left) and the turbulent (right) solution.  $I$  and  $D$  are the total energy input and dissipation normalized with those of a laminar state. The segment of the turbulent (green) orbit exhibiting an approach to the periodic solution is colored red.

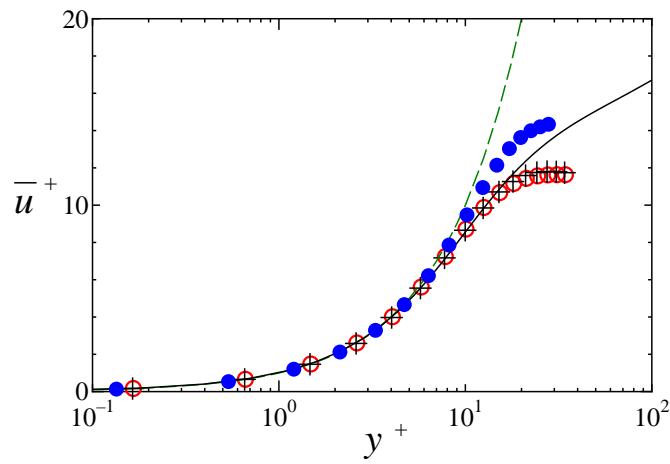


Figure 6: Comparison of the normalised mean velocity profiles between the Kawahara & Kida (2001) time-periodic and turbulent flows. The mean stream-wise velocity  $\bar{u}^+ = \bar{u}/u_\tau$  is shown as a function of the distance from the wall  $y^+ = yu_\tau/\nu$ .  $\circ$ , the vortex-dominated periodic solution at  $Re_\tau = 34$  representing regeneration cycle;  $\bullet$ , the streak-dominated gentle periodic solution at  $Re_\tau = 28$ .  $+$ , the turbulent solution for the same condition; —, the turbulent solution for plane Poiseuille flow at  $Re_\tau = 590$  (Moser et al. 1999). - - - -, the laminar solution  $\bar{u}^+ = y^+$ .

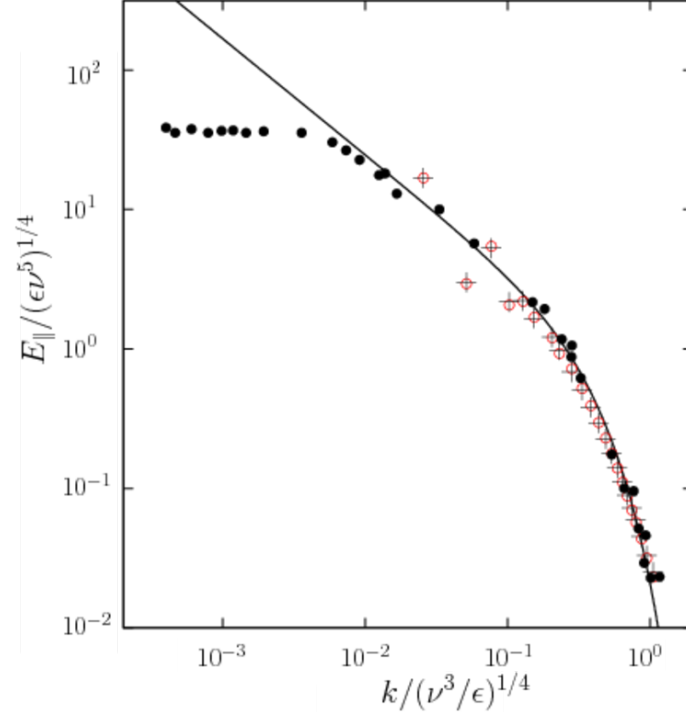


Figure 7: One-dimensional longitudinal energy spectrum  $E_{\parallel}$  for the van Veen et al. (2006) periodic solution in Kida–Pelz high-symmetric flow. The lateral and longitudinal axes are normalised by  $(\nu^3/\epsilon)^{1/4}$  and  $(\epsilon\nu^5)^{1/4}$ , respectively.  $\circ$ , the periodic state of high-symmetric flow at  $R_{\lambda} = 67$ ;  $+$ , the turbulent state of high-symmetric flow;  $\bullet$ , experimental data of homogeneous shear turbulence at  $R_{\lambda} = 130$  taken from Champagne et al. (1970). —, the high- $R_{\lambda}$  asymptotic form derived theoretically by the sparse direct-interaction approximation (Kida & Goto 1997).

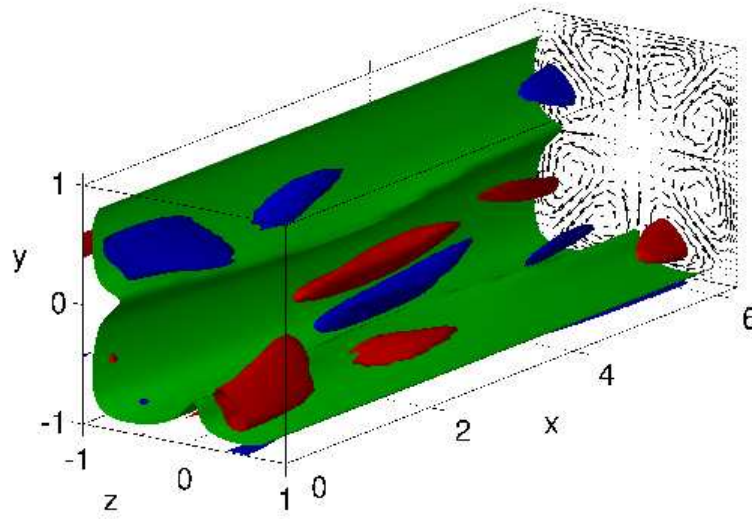


Figure 8: Travelling wave in pressure-driven square-duct flow (Uhlmann et al. 2010). The upper-branch solution at Reynolds number  $Re \equiv Uh/\nu = 1404$  ( $U$  and  $h$  being the bulk mean velocity and the duct half-width, respectively) and streamwise period  $L_x/h = 2\pi$  is shown by means of surfaces of constant values of the total streamwise velocity  $u = 0.55 \max(u)$  (sheet-like structure near the walls, green color) and of the streamwise vorticity at  $\pm 0.65 \max(\omega_x)$  (tubular structures, blue/red color). The surfaces are cut away on one side of a diagonal of the duct cross-section for improved clarity. Mean secondary flow vectors are projected upon the back plane of the graph. Flow is toward positive  $x$ .

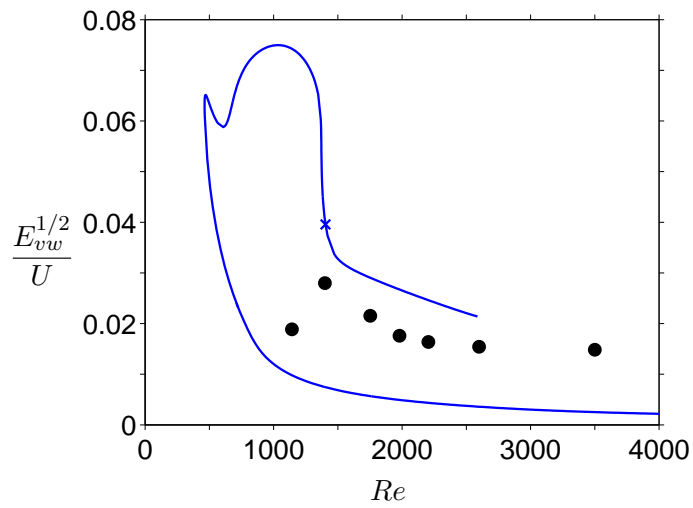


Figure 9: The intensity of the mean secondary flow  $E_{vw}^{1/2}$  (where  $E_{vw}$  is the energy of the streamwise-averaged flow in the cross-section, defined in an integral sense) for the duct flow travelling waves of Uhlmann et al. (2010), normalized by the bulk velocity  $U$  and shown as a function of the Reynolds number. The blue solid line (—) connects solutions at constant streamwise period  $L_x/h = 2\pi$ ; the cross (×) corresponds to the flow field visualized in figure 8. The closed symbols (•) are for long-time averaged turbulent flow in domains with length  $L_x/h \approx 4\pi$  (Uhlmann et al. 2007).

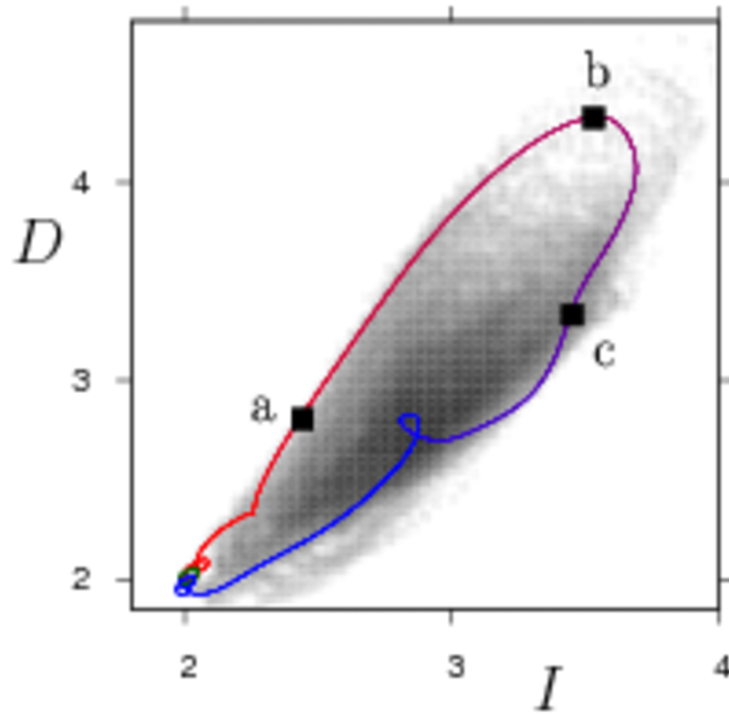


Figure 10: Projection of the orbit homoclinic to the gentle periodic solution (shown in green) in plane Couette flow at  $Re = 400$  onto the energy input  $I$  and the dissipation rate  $D$ , normalised by their value in laminar flow (van Veen & Kawahara 2011). The piece of orbit leaving the gentle periodic solution is shown in red and the one approaching it in blue. In the background, the PDF (Probability Density Function) of transient turbulence is shown in gray scale. The labels **a–c** correspond to the snap shots in Figure 11.

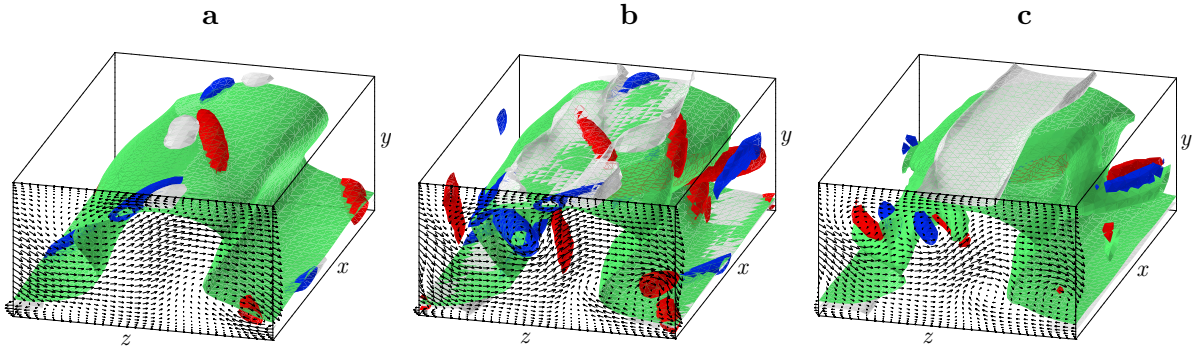


Figure 11: Visualizations of flow structures in one periodic box  $L_x \times 2h \times L_z$  at three phases on the orbit homoclinic to the gentle periodic solution in plane Couette flow at  $Re = 400$  (van Veen & Kawahara 2011), labeled as in Figure 10. The green, corrugated isosurfaces of the null streamwise ( $x$ ) velocity represent a streamwise streak. Red and blue objects are isosurfaces of  $0.4\rho(U/h)^2$  for the Laplacian of the pressure, and denote the vortex tubes of the positive and negative streamwise-vorticity component. Gray isosurfaces show the local energy dissipation at 20 times the value of laminar dissipation. Cross-stream ( $y, z$ ) velocity is also shown in the plane  $x = 0$ . The flow symmetry suggests that cross-stream velocity in the plane  $x/h = L_x/2$  is given by the reflection of that in the plane  $x = 0$  in the spanwise ( $z$ ) direction.